



HAL
open science

The power of the physical fabric of mudstone in creating trace fossil like redoximorphic features, case study from the late Eocene, Sirt Basin

Ashour Abouessa, Philippe Düringer, Jonathan Pelletier

► To cite this version:

Ashour Abouessa, Philippe Düringer, Jonathan Pelletier. The power of the physical fabric of mudstone in creating trace fossil like redoximorphic features, case study from the late Eocene, Sirt Basin. *Journal of African Earth Sciences*, 2020, 170, pp.103931. 10.1016/j.jafrearsci.2020.103931 . insu-02919338

HAL Id: insu-02919338

<https://insu.hal.science/insu-02919338>

Submitted on 22 Aug 2020

HAL is a multi-disciplinary open access archive for the deposit and dissemination of scientific research documents, whether they are published or not. The documents may come from teaching and research institutions in France or abroad, or from public or private research centers.

L'archive ouverte pluridisciplinaire **HAL**, est destinée au dépôt et à la diffusion de documents scientifiques de niveau recherche, publiés ou non, émanant des établissements d'enseignement et de recherche français ou étrangers, des laboratoires publics ou privés.

Journal Pre-proof

The power of the physical fabric of mudstone in creating trace fossil like redoximorphic features, case study from the late Eocene, Sirt Basin

Abouessa Ashour, Durringer Philippe, Pelletier Jonathan



PII: S1464-343X(20)30182-5

DOI: <https://doi.org/10.1016/j.jafrearsci.2020.103931>

Reference: AES 103931

To appear in: *Journal of African Earth Sciences*

Received Date: 6 January 2020

Revised Date: 5 June 2020

Accepted Date: 9 June 2020

Please cite this article as: Ashour, A., Philippe, D., Jonathan, P., The power of the physical fabric of mudstone in creating trace fossil like redoximorphic features, case study from the late Eocene, Sirt Basin, *Journal of African Earth Sciences* (2020), doi: <https://doi.org/10.1016/j.jafrearsci.2020.103931>.

This is a PDF file of an article that has undergone enhancements after acceptance, such as the addition of a cover page and metadata, and formatting for readability, but it is not yet the definitive version of record. This version will undergo additional copyediting, typesetting and review before it is published in its final form, but we are providing this version to give early visibility of the article. Please note that, during the production process, errors may be discovered which could affect the content, and all legal disclaimers that apply to the journal pertain.

© 2020 Published by Elsevier Ltd.

The power of the physical fabric of mudstone in creating trace fossil like redoximorphic features, case study from the late Eocene, Sirt Basin

Abouessa Ashour^a, Düringer Philippe^a, Pelletier Jonathan^b

a: Institut de Physique du Globe de Strasbourg (IPGS), UMR 7516, Université de Strasbourg (UdS), École et Observatoire des Sciences de la Terre (EOST), Centre National de la Recherche Scientifique (CNRS), Bâtiment de Géologie, 1 rue Blessig, 67084 Strasbourg Cedex, France

b: TOTAL, Technical Centre, Avenue Larribau, 64018 Pau Cedex, France

Abstract

This article presents complex paleo-pedoturbation features, preserved in a massive mudstone stratum belonging to a siliciclastic sequence in the upper Eocene. The outcrop of these turbations presents an intricate network of iron oxide in semi tubular forms. The mudstone to which these structures are restricted is lithologically similar to other mudstone beds, below and above it in the sequence. In contrast, it presents more paleo-pedogenic features.

Attributing these tubular structures to a specific burrow is difficult for two reasons: the apparent similarities in morphology to numerous trace fossils coupled with the absence of diagnostic excavation-locomotion proxies, as well as the lack of any faunal or floral body fossils in the parent mudstone. Moreover, these structures do not convincingly conform to the simplified image documented in numerous publications for fossil roots.

Taking into account the exclusive, physicochemical properties of the clay rich rocks (shrink-swell behaviour, erratic permeability and cation-exchange capacity), this article provides potential evidence that such trace fossil-like features could, alternatively, be produced by abiotic redox processes without pre-existing faunal or floral predecessors. Regardless of the extent to which the provided justifications are acceptable, they might increase awareness as to just how treacherous trace fossil identification can be. The studied case draws attention to the fact that, in mudstones, the dividing line between valid and spurious trace fossils can be very subtle. It also assists in better recognition of paleosol features in mudstones.

Keywords: mudstone fabric, paleosols, redox features, trace fossils, tubular forms, Fe-oxides

1. Introduction

The morphological pattern of redoximorphic features in paleosols, and sedimentary rocks in general, are controlled by the pre-existence of either physical fabric or biogenic fabric. Such abiotic or biotic templates are overprinted by the accumulation of iron or other oxides to preserve the pre-existing morphology. The attribution of the redoximorphic accumulation of tubular (or similar) structures to pre-existing roots or burrows became almost spontaneous because of its ubiquity. In fact, ascribing any almost-tubular morphologic features to presumed, formerly existing roots or burrows is not always correct and, thus, might cause false geological interpretations. In clay dominated strata, with their particular textural and geochemical properties, morphogenic features attributed to pre-

40 existing physical textures and fabrics have received little attention and appear to have been under-
41 estimated.

42 The Late Eocene outcrop in the Sirt Basin (Fig. 1a) presents a case study where structures that
43 were previously interpreted as trace fossils (Wight, 1980; Abouessa et al., 2012) might also be
44 ascribed to physical rather than biogenic ancestors. In soils and sediments, complex Fe-oxide
45 precipitation patterns produced by porewater/rock interactions result in morphological features that
46 reflect the internal structures of the host rocks (Muller and Bocquier, 1986; Goldenfeld et al., 2006;
47 Chan et al., 2007; Barge et al., 2011). The drainage capacity (permeability) of sediments is an essential
48 controlling factor in the distribution of oxide accumulation (Gasparatos et al., 2002; Kraus and
49 Hasiotis, 2006; Brierley et al., 2011). Accordingly, the pattern of solute circulation and deposition
50 would strongly differ from muddy to sandy sediments, based on their drainage capacity.

51 In sandstones with isotropic hydraulic conductivity, redox features are initiated as simple
52 structureless nodules that then become concretions with uniform, concentric structures (Brewer, 1964;
53 Veneman et al., 1975; Gasparatos, 2012). Their shape is controlled by the texture of the sediments.
54 Their precipitation is initiated around physical or biological nuclei (Allison, 1988; Allison and Duck,
55 1990; Trewin, 1992; Martinez, 1996; Richter et al., 2007). If physicochemical conditions allow for
56 continuous precipitation, concretions evolve into distinctly shaped, variant and uniform, self-
57 organising Liesegang patterns (Kessler and Werner, 2003; Wang et al., 2015). Thus, physicochemical
58 precipitation could accumulate ‘unexpectedly’ variable features by overprinting the pre-existing
59 physical fabric of the sediments. For instance, sand pipes (Thompson and Stokes, 1970) result from
60 iron minerals precipitating out of ground water as it moves through the rock. Tubular structures of iron
61 oxide at Rio Tinto (Barge et al., 2016) form through self-assembly via an abiotic mechanism involving
62 templated precipitation around a fluid jet. In fact, the extent that physicochemical morphological
63 features can reach is best given by cave deposits (speleothems and helictites) (Hinman, 1988; Aharon
64 et al., 2006). These are precipitated on the cave walls during the seepage of water from rock into the
65 air. Therefore, considering the highly variable temporal and spatial interactions between all textural
66 and environmental factors, the precipitation pattern would be unexpectedly delicate.

67 Given that the permeability of sediments is a major factor in the passage of cation-carrying
68 solutions, the accumulation trends will vary unevenly, even in the same sediments. In contrast to the
69 well-organised redox features given by sandstones, mudstones would host features that reflect their
70 particularities due to their different physicochemical properties. These properties include shrink-swell
71 behaviour, the cation-exchange capacity (Muller and Bocquier, 1986; Smith et al., 2008; Kvoda et al.,
72 2016), and the anisotropic “non-Darcian” permeability (Mitchell et al., 2005; Wang et al., 2018).
73 Permeability in mudstones is very low and heterogeneous compared to that of sand and siltstones.
74 Solute transport and precipitation in mud is more influenced by secondary permeability, such as that
75 produced by dehydration cracks and micrograin rearrangement during the formation and alteration of

76 soil peds (through pelitoclastesis) (Bouma et al., 1977; Zhang and Karathanasis, 1997; Wetzel and
77 Einsele, 1991; Canton et al., 2001; Mondol et al., 2008; Moussavi-Harami et al., 2009).

78 In this succession (Fig. 1b), among many lithologically-similar mudstone strata, the studied
79 stratum (1–2 m in thickness; Fig. 1c) preserves exclusive paleo-pedogenic features. In addition to the
80 initial redoximorphic mottling and localised Fe-oxide accumulations, pedoturbation structural forms
81 that largely resemble the trace fossil *Thalassinoides*. These structures are generally presented as
82 crowded tubular and semi-cylindrical accumulations of iron oxides. Their morphology makes it hard
83 to exclude biogenic templates. Their architecture is, therefore, either unusually well-organised or very
84 poorly shaped, to be ascribed to floral or faunal predecessors. In fact, there are always delicate
85 elements that do not concord with a presumed biogenic ancestry, and other elements that support
86 physical templates. An argument will be presented by this article. The aim is not to completely deny
87 the trace fossil origin but to highlight an alternative interpretation that might be realistic in the case of
88 clay-rich sediments.

89

90 2. The geological context

91 Among several massive and differently-fractured mudstone strata, the studied paleo-
92 pedoturbations are restricted to, and are characteristic of, one stratum. This stratum is embedded in the
93 upper, fluvially-dominated, part of an 80 m succession of thinly stratified siliciclastic rocks called the
94 New Idam Unit (Abouessa et al., 2012). Each of the mudstone beds in this unit is ~1–2 m thick,
95 bearing, in most cases, erosive upper and gradational lower contacts with the sandstones. The entire
96 unit was deposited in a regressive estuary. Marine indicators dominate the lower part of the sequence,
97 while terrestrial indicators dominate the upper part (Wight, 1980; Abouessa et al., 2012, 2015). This
98 fact is given by the prevalence of diagnostic biogenic indications (traces, fauna, flora) with which the
99 New Idam Unit is exceptionally crowded (Savage, 1970; Wight, 1980; Rasmussen et al., 2008;
100 Abouessa et al., 2012, 2015). Assemblages of sedimentary and biogenic structures, as well as fossil
101 fauna and flora, indicate that a tropical-subtropical climate was prevailing at the time of deposition in
102 the Late Eocene (38–39 Ma) (Jaeger et al., 2010a, b). In the sandstone strata, fossil root traces are
103 evident and terrestrial bioturbation structures are ubiquitous. Contrastingly, in the mudstone beds, the
104 paleo-pedogenesis is less developed, being restricted to discolouration, slickensides, shrink-swell
105 cracks, pelitoclastesis and, possibly, roots.

106 The geological context indicates that the sand-siltstone beds are channel and inter-channel flat
107 deposits. The mudstones are interpreted in the lower part of the New Idam Unit as being intertidal
108 lagoons. This is evidenced by the embedded shallow marine molluscs and the diagnostic sedimentary
109 tidal structures (Abouessa et al., 2012, 2015). In the upper part, where the host mudstone stratum is
110 located (Fig. 1b, c), mudstone beds are largely attributed to shallow, fresh water lakes. This is proven,

111 not only by the domination of successive pedogenically-altered layers (with terrestrial fossils and trace
112 fossils) but, also, by the complete disappearance of marine fossils.

113 In a broader sense, the colour of the mudstone beds in the terrestrial part lies in the spectrum
114 of light green to light greenish-grey. The latter is the colour of the dominating matrix of the host mud,
115 thus attesting to poor drainage conditions (e.g. Kraus, 1998). In comparison, a light bluish-green
116 colour prevails in the lower, marine-dominated mudstones. The clay minerals forming the mudstones
117 are predominantly kaolinite, chlorite and montmorillonite (Wight, 1980; Vasic and Sherif, 2007).

118

119 **3. Description of the host mudstone**

120 All of the mudstone beds, including the one hosting the studied pedoturbation, are water-lain
121 suspension deposits (originally water-saturated). No syndimentary structures are observed, nor are
122 there any indications of compaction or dissolution. From one mudstone bed to another, characteristic
123 dehydration (shrink-swell) cracks/fractures show the character of the clay-rich vertisols (e.g.
124 Duchaufour, 1982; Kraus and Aslan, 1993; Soil Survey Staff, 1998) (Fig. 2a–h). These are of a
125 remarkably variable intensity, dimension and orientation pattern. Mottling predominantly re-occurs as
126 whitish, light-grey spots and patches as well as pale yellow to light brown pigmentation along joints
127 and slickenside faces (Fig. 2d). Locally, these can also be purple and, more rarely, red. The fractures
128 can appear to be regular and irregular, open and closed. They are millimetres to centimetres apart and
129 up to several centimetres long. The more striking fracture orientations are vertical to subhorizontal,
130 straight and irregular. Subordinate finer cracks, in-between the main fractures, create patterns that are
131 variable from one site to another.

132 The fractures are particularly more intense in the host mudstone and are more variably
133 oriented. Diagonal (Figs. 2h, 3a, b) and circular fractures are obvious here, compared to other
134 mudstone beds. Interlocking cracks are common, with variable dimensions, simple and composite
135 structures, subcircular and circular in shape. These are organised in a similar manner (Fig. 3c–e) and
136 are better developed with increasing depth. Similar concentric cracks in mud are described in Ollier
137 (1971) and Lakshmikantha (2009). Together with the other paleo-pedogenic processes, the influence
138 of fracturing in the fabric of this mudstone seems overriding. Vermicular structures (Retallak, 1983)
139 are also present (Fig. 3f).

140 Like the shrink-swell fractures, mottling and Fe-coatings are also more common in the host
141 mudstone. These occur as subcircular spots and discolouration patches, ubiquitously scattered in the
142 matrix. Among others, common lath-shaped forms are found, either in isolation or in continuity with
143 the brown Fe-oxide cumulate (e.g., Fig. 3a, b). All of these aspects are also acknowledged as common
144 criteria in vertisols (e.g. Driese and Foreman, 1992; Mack et al., 1993; Driese et al., 2000; Miller et al.,
145 2010; Kovda et al., 2016).

146

147 **4. Description of the hosted structures**

148 In a broad sense, the studied iron oxide turbations are exhibited as a network of reticulated and
149 solitary, delicately and poorly shaped semi-tubular structures. Overall, they resemble the trace fossil
150 *Thalassinoides* and fossil roots, to a lesser extent. They constitute finger-sized, 1–2 cm tubules and
151 larger semi-cylindrical regular and irregular shafts, 5–15 cm in diameter (Fig. 4a, b). Small tubules are
152 commonly a few cm long and are angularly attached together. They appear to be longer when
153 longitudinally joined; very narrow separation cracks can occasionally be discerned. The large tubules
154 (shafts) are up to 35 cm long. In an intermediate horizon, many of them are strictly parallel (Fig. 4c–f).
155 The small tubules densely dominate, but are not restricted to, the top 30–40 cm horizon. The shafts are
156 less dense in the lower part of host bed but neither penetrate the subjacent sandstone nor reach the top
157 of the host. The two forms (tubules and shafts) interlock together (Fig. 4b, d) in the intermediate zone,
158 30 to 70 m below the top of the host bed. In addition to the (considerably defined) tubular forms,
159 morphologically different Fe-oxide structures with angular edges and straight outlines (Fig. 5a–c), are
160 adjacently associated.

161 The interior (filling) of all these structures is composed of massive muddy materials,
162 dominated by iron oxides. The prevailing colour is brown-yellow which is indicative of goethite
163 (Duchaufour, 1982; Schwertmann and Taylor, 1989; PiPujol and Buurman, 1994; Gasparatos et al.,
164 2004). The overall texture is similar to the ambient sediments. The outer surfaces are smooth, knobby,
165 and scaly, with no special textural ornamentations. There are locations in the parent mudstone where
166 the adjacent mud fabric exhibits a fracturing pattern with identical textural and orientation aspects to
167 that of the hosted structures (Fig. 5a–d).

168 The colours preserved by all the morphoforms are not restricted to brown-yellow. Pale yellow,
169 light to dark brown and whitish grey are also incorporated. Forms preserving a patchwork of these
170 colours are not exceptional (Figs. 4c–f; 5b, d). Structures where the colour gradually changes from
171 whitish grey to brown or yellow are common. Abrupt colour contact with the greenish matrix seems to
172 prevail (Fig. 5a, b). Halos of lighter colour shades surrounding larger structures are not uncommon.
173 Notably, in many cases these halos resemble the shape and the dimensions of the adjacent tubules
174 (Fig. 5c, d).

175 The cross-sectional area of the small tubules is commonly semi-circular and flattened, with
176 their two dimensions being occasionally changeable along their long axis. Despite the organisational
177 pattern of the network, cross-cutting between individuals is not evident, although they give the
178 appearance of having intersected. Meeting points are dominantly angular rather than curved (Fig. 5d,
179 e). Remarkably distinctive cross-hatched patterns (Fig. 5e) are re-occurring.

180 Closer to the base of the host bed, the shafts contrastingly prevail over the small tubules,
181 which became scarce and solitary. Compared to those slightly above, the shafts here are evidently

182 circular, with their outer surface (crust) having become very unevenly agglomerated and/or coarsely
183 botryoidal (Fig. 6a, b). The interior consists of muddy materials of a greenish brown colour, grading
184 out to dark brown at the resistant crust. Besides this, the outcrop at this location presents a common
185 case where the interior of the shafts is composed of several smaller tubules with a circular cross-
186 sectional area, made distinctive by their internal, concentric bands (Fig. 6b, c). Smaller tubules also
187 grow adjacently, attached (Fig. 6a, b) or detached (Fig. 6b, c) from the shafts. They may extend for a
188 few tens of centimetres (Fig. 6d) with no change in their diameter.

189

190 **5. Discussion**

191 The principle aim of this chapter is to test the possibility of the pre-existence of physical,
192 rather than biological, templates for the described redoximorphic features. With respect to the
193 morphology alone, the hypothesis of a physical signature would seem unlikely. This is because
194 geologists used to spontaneously attribute such a network of tubular forms to biological origins, and
195 this was usually true. This discussion attempts to orient attention towards the influence of the physical
196 fabric and emphasizes the role of physicochemical (abiotic) processes on the production of such trace
197 fossil-like structures. Two lines of justification are worth examining: (i) the contradictions presented
198 by these structures if they are of biotic origin; (ii) the extent to which abiotic physical processes can
199 produce such figures on their own.

200 Firstly: considering morphology, it is almost impossible to provide solid evidence that
201 completely refutes the former existence of burrows created by crustaceans and annelids, or roots. All
202 of those can leave behind a similar network (e.g. Bromley and Frey, 1974; Howard and Frey, 1984;
203 Seilacher, 2007; Hasiotis and Mitchell, 1993; Monaco, 2000; Hasiotis and Bourke, 2006; Moh et al.,
204 2015). Apart from the morphology, these Fe-oxide structures are barren of any strict evidence of a
205 biogenic origin. The known traits concerning the mode of preservation of roots (Klappa, 1980; Jaillard
206 et al., 1991; Hasiotis, 2002; Kraus and Hasiotis, 2006; Genise et al., 2004; Gregory et al., 2004;
207 Nascimento et al., 2019) is not fulfilled by those structures. Despite the good preservation of such soft
208 sediments (Buatois and Mángano, 2004), no evident roots, moulds or casts are preserved, although
209 they are evident in other strata, above and below. Carbonised remains of roots and central root canals
210 are absent and secondary roots (branching/ root hairs) are not detected either. The characteristic
211 tapering downward of root morphology cannot be considered to be evident here. Moreover, the length
212 of the individual tubules is a few centimetres and so the length to width ratio is too large to be
213 confidently attributed to the known burrow-making organisms, neither match with those of roots. The
214 sharp angle of tubule attachment enhances this aspect. It seems to be too angular to be ascribed to the
215 burrowers producing similar tubular morphology. Known evidence for burrowing organisms'
216 locomotion, such as scratch marks and wall linings, are totally absent.

217 In fact, the halos (such as the ones in Figure (5d)) that resemble the Fe-oxide tubules, could be
218 considered as the initial step of producing these tubules away from any biological guidance. Here, the
219 stains affect the intact, non-turbated, matrix. Such localised iron oxide precipitation in mudstones is
220 thought to be initiated along microscopic fractures and/or in localised sites of increased permeability
221 (Vepraskas, 1994; Driese et al., 1995; Hildenbranda and Uraib, 2003; Gasparatos et al., 2004).
222 Refutation of faunal/floral activities preceding the iron oxide accumulation is, thus, suggested by the
223 lack of any marks or indications of excavation and root penetration. Concerning the semi-cylindrical
224 bodies, the angle of inclination, together with the parallelism, does not fit with that of biogenic
225 activities. Furthermore, the texture and the internal structure of the tubules are identical to that of the
226 ambient mudstone (Fig. 5a–d). There is no external material introduced from the superjacent
227 sandstone.

228 Secondly: to what extent could abiotic physical predecessors provide the template for such Fe-
229 oxide figures on their own? The essential elements in this regard are suggested by the exclusively
230 abiotic (physical as well as chemical) paleo-pedogenic processes that eventually acted on the various
231 mudstone beds in the succession. The network of dehydration cracks reflects the response to physical
232 processes (Einsele, 1983; Bland and Rolls, 1998; Mondol et al., 2008). The iron oxide's pigmentation
233 and thicker accumulations along and around the physical surfaces (e.g. Fig. 2d) are related to the
234 chemical processes. In paleosols with similar vertic properties, these processes are related to the
235 repeatability of wetting/drying climatic cycles (Sridharan and Allam, 1982; Canton et al., 2001;
236 Kishné et al., 2009; Tang et al., 2011; Kovda et al., 2016) which is able to significantly alter the
237 original fabric. Climatic conditions, in combination with the prevailing geochemical factors, are
238 responsible for producing different soil morphologies (Brewer, 1976; Martinez, 1996; Wright, 1995;
239 Breemen and Buurman, 2002). Accordingly, the host mudstone, compared to the other mudstone beds
240 in the sequence, must have been subjected to relatively prolonged periods of pedogenesis that resulted
241 in morphoforms similar to trace fossils. Rectangular rhombic, vermicular and concentric fabrics (Fig.
242 3) are among those physical forms that are particularly exhibited by the mudstone. The overprinting of
243 these fabric forms is analogous to the overprinting of biogenic (faunal or floral) fabrics (Veneman et
244 al., 1975; Vepraskas, 1994).

245 Based on the preserved mudstone fabric, the quadrant geometrical forms, with their sharp
246 rectangular edges (Fig. 5a, for instance), undoubtedly attest to the physical soil fabric being
247 overprinted. These are simply slickensided masses of mudstone, coated by goethite, concentrated
248 along the boundaries. Similarly, the parallel (semi-cylindrical) forms are due to goethite accumulation
249 around differently fabricated mud masses. Besides their perfect parallelism, in-depth examination
250 reveals that most cylinders are incompletely circular. There is always one side that is straight enough
251 to be attributed to a burrow rather than to a fracture wall, and the facing side is usually a parallel
252 fracture that, illusively, appear as part of the cylinder (Fig. 4e). The unexcavated interior which is
253 texturally identical to the ambient mud, supports this view. It is worth comparing the 'certain'

254 cylindrical shape of the decapod trace fossil (Abouessa et al., 2015) found in the sandstone beds, both
255 sub and superjacent to the host mudstone.

256 Since there is no clear Fe-source above and below the hosting bed, the iron must have been
257 provided by the clay minerals comprising the mudstone, which are characterised by their iron content
258 and their high cation-exchange capacity (Dasog et al., 1988; Soil Survey Staff, 1998; Manceau et al.,
259 2000; Brierley et al., 2011; Kvoda et al., 2016). Iron removed from clay via reduction processes leaves
260 behind whitish grey patches (Fig. 3a, b), displaced through cracks, and re-deposited at first contact
261 with oxygenated sites (Schwertmann and Taylor, 1989; Schwertmann, 1993; Vepraskas, 1994;
262 Beverly et al., 2018). Further growth and shaping of the iron precipitate are then controlled by the
263 local fabric, the local permeability, and the availability of the Fe-charged solutes. Comparable cases
264 and details about the mechanism are best illustrated in Buurman (1975), Retallack (1983), PiPujol and
265 Buurman (1994), Drles et al. (1995), and Beverly et al. (2018).

266 The composite shafts, with their concentric tubules, are then explained by the concentric
267 cracks presented by the ambient mudstone (Fig. 3c–e), which provide solute conduits as well as
268 accumulation sites. Here, the shafts essentially overprinted the crack rings presented by the mud.
269 Practical proof is given by the half circular accumulations, such as those shown in Figure (7a, b)
270 where the iron oxide precipitate has efficiently overprinted the circular cracks. The circular forms here
271 are not complete because precipitation has stopped, either due to insufficient solution or because the
272 precipitation had been deviated vertically in response to the imperfect drainage. Precipitation would
273 continue preferentially vertically, along a given fracture, when impeded from lateral growth (Yuen et
274 al., 1998; Rayhani et al., 2008; Li et al., 2009). The internal tubules, with their concentric bands,
275 simulate the smaller circular rings. Some of them grow independently while others grow attached to
276 the large shafts. The tendency of iron oxides precipitate to form tubular bodies (Ambrosi and Nahon,
277 1986; Muller and Bocquier, 1986; Gaiffe and Kubler, 1992; Sadek and Sultan, 2011; Berge et al.,
278 2016) can be recalled for this location. This can be further ‘guesstimated’ by Figure (7c), where the
279 reduction and oxidation have occurred adjacently on the fractured mudstone masses, of which the
280 matrix is non-bioturbated. Further explanations and comparable cases are given by Brewer (1976),
281 Arshad and Arnaud (1980), Pipujol and Buurman (1994), Vepraskas (1994) and Kessler and Werner
282 (2003).

283 Concerning the networks of finger-sized tubules, they might be hardly attributable to the
284 relatively more intense fracture networks. Nevertheless, this hypothesis might be considered
285 acceptable, if one takes into account the fact that, at a certain stage of pedogenesis, a vermicular
286 structure (Figs. 2g, 3f), similar to these tubes, had been fabricated by the combination of the fractures
287 and the mud aggregation. Thus, dehydration cracks, in combination with pelitoclastesis (Wetzel and
288 Einsele, 1991; Canton et al., 2001), are probably able to produce such tubular fabrics that are later
289 impregnated by Fe-oxides. Actually, the cross hatched pattern in Figure (5e) might be comparable to
290 the rhombic organisation in Figure (2h). This speculation would be considerably more reliable if one

291 considers that such fractures were initiated as microfractures (Cescas et al., 1970; Kranz, 1983; Kishné
292 et al., 2009) and expanded along with the repeated wetting/drying seasons and the concomitant Fe-
293 oxide growth, to result in the present image.

294

295 **6. Conclusion**

296 This article emphasises the similarity of the redoximorphic features created by inorganic
297 processes to those created as bioturbations in mudstones. It is evident that the variations in
298 paleoclimatic conditions have led to striking differences in the physical fabric of the clay-rich
299 sediments. The tubular forms of iron oxides are exceptionally manifest in the mudstone, which
300 obviously preserves greater degrees of redox mottling and intensity of the dehydration fractures. The
301 proliferation of these abiotic pedogenic features, compared to those of other mudstones, reflects and
302 records the influence of relatively more repetitive 'wetting/drying' seasons. Therefore, this suggests
303 that subtropical paleoclimatic depositional conditions prevailed in the area during the Late Eocene.

304 Emphasis on the recognition of the physical fabric of mudstones will not only help in
305 predicting paleoclimate but also in reducing the risk of geological misinterpretation. Since the physical
306 fabric could lead to the production of redox patterns resembling those of the biogenic fabric, the
307 spontaneous interpretation of tubular redoximorphic features in mudstones as trace fossils is not
308 necessarily correct. Being aware of the ubiquity and patterning of the physical paleo-pedogenic
309 features will certainly help in avoiding erroneous interpretations. Additionally, by attributing the
310 occurrence of these features to the influence of climatic conditions, physical redoximorphic features
311 become a very useful tool for recognising emersion surface sequence boundaries.

312

313 **Acknowledgments**

314

315 Thanks firstly go to program PAUSE for the financial support of a research job for Mr.
316 Abouessa at University of Strasbourg, and for the University of Strasbourg (UDS/EOST) for the
317 adoption of the study Project. Special thanks go to M. Schuster for his very critical and exciting
318 comments. J.-F. Ghienne's contribution was, as well, very constructive. Finally, the corrections
319 provided by the reviewers to improve the manuscript are highly appreciated, those made by M. Alfred
320 Uchman are greatly refined the original version.

321

322 **References**

323

- 324 Abouessa, A., Pelletier, J., Düringer, Ph., Schuster, M., Schaeffer Ph., Métais, E., Benammi, M., Salem, M., Hlal,
325 O., Brunet, M., Jaeger, J.-J., Rubino, J.-L., 2012. New insight into the stratigraphy and sedimentology of the Dur
326 At Talah escarpment (Eocene–Oligocene, Sirt Basin, Libya). *Journal of African Earth Sciences* 65, 72–90.
- 327 Abouessa, A., Düringer, Ph., Schuster, M., Pelletier, J., 2015. Crayfish fossil burrows, a key tool for
328 identification of terrestrial environments in tide-dominated sequence, Upper Eocene, Sirt Basin, Libya. *Journal*
329 *of African Earth Sciences* 111, 335–348.
- 330 Ambrosi, J.P., Nahon, D., 1986. Petrological and geochemical differentiation of lateritic iron crust profiles.
331 *Chemical Geology* 57, 371–398.
- 332 Arshad, M.A., Arnaud, R.J., 1980. Occurrence and characteristics of ferromanganiferous concretions in some
333 Saskatchewan soils. *Canadian Journal of Soil Sciences* 60, 685–695.

- 334 Barge, L.M., Hammond, D.E., Chan, M.A., Potter, S., Petrusk, J., Nealson, K.H., 2011. Precipitation patterns
 335 formed by self-organizing processes in porous media. *Geofluids* 11, 124-133.
- 336 Barge, L.M., Cardoso, S.S., Cartwright, J.H., Doloboff, I.J., Flores, E., Macías-Sánchez, E., Sainz-Díaz, C.I.,
 337 Sobrón, P., 2016. Self-assembling iron oxyhydroxide/oxide tubular structures: laboratory-grown and field
 338 examples from Rio Tinto. *Proceedings of the Royal Society* 472, 1–19.
- 339 Beverly, E.J., Lukens, W.E., Stinchcomb, G.E., 2018. Paleopedology as a Tool for Reconstructing
 340 Paleoenvironments and Paleoecology. D.A. Croft et al. (eds.): *Methods in Paleoecology: Reconstructing*
 341 *Cenozoic Terrestrial Environments and Ecological Communities, Vertebrate Paleobiology and*
 342 *Paleoanthropology* p 151–183.
- 343 Bland, W., Rolls, D., 1998. *Weathering – An introduction to the scientific principles*. Arnold Publishers,
 344 London, 280 p.
- 345 Brewer, R., 1976. *Fabric and Mineral Analysis of Soils*. Krieger Publ. Co., Huntington, New York. 482 p.
- 346 Brierley, J.A., Stonehouse, H.B., and Mermut, A.R., 2011. Vertisolic soils of Canada: Genesis, distribution, and
 347 classification. *Canadian Journal of Soil Sciences* 91, 903–916.
- 348 Bromley, R.G., Frey, R.W., 1974. Redescription of the trace fossil *Gyrolithes* and taxonomic evaluation of
 349 *Thalassinoides*, *Ophiomorpha* and *Spongeliomorpha*. *Bulletin of Geological Society of Denmark* 23, 311–335.
- 350 Bouma, J.A., Jongerius, A., Boersma O., Jagger, A., 1977. The function of different types of macropores during
 351 saturated flow through four swelling soil horizons. *Soil Science Society of America Journal* 41, 945–950.
- 352 Breemen, V.N., Buurman, P., 2002. *Soil Formation, Second Edition*, 404 P.
- 353 Buatois, L.A., Mángano, M.G., 2004. Animal-substrate interactions in freshwater environments: applications of
 354 ichnology in facies and sequence stratigraphic analysis of fluvio-lacustrine successions. *Geological Society of*
 355 *London, Special Publications* 228, 311–333.
- 356 Buurman, P., 1975. Possibilities of paleopedology. *Sedimentology* 22, 289–298.
- 357 Cescas, M.P., Tyner, E.H., Harner, R.S., 1970. Ferromanganiferous soil concretions: A scanning electron
 358 microscope study of their micropore structures. *Soil Science Society of America Proceedings* 34, 641–644.
- 359 Chaosheng Tang, Yu-Jun Cui, Bin Shi, Anh Minh Tang, Chun Liu, 2011. Desiccation and cracking behavior of
 360 clay layer from slurry state under wetting-drying cycles. *Geoderma* 166, 111–118.
- 361 Chan, M.A., Ormö, J., Park, A.J., Stich, M., Souza-Egipsy, V., Komatsu, G., 2007. Models of iron oxide
 362 concretion formation: field, numerical, and laboratory comparisons. *Geofluids*, 7, 356–368.
- 363 Duchaufour, P., 1982, *Pedology*: London, George Allen & Unwin Ltd., 448 p.
- 364 Dasog, G.S., Acton, D. F., Mermut, A. R. and de Jong, E., 1988. Shrink-swell potential and cracking in clay soils
 365 of Saskatchewan. *Canadian Journal of Soil Sciences* 68, 251–260.
- 366 Driese, S.G., Foreman, J.L., 1992, Paleopedology and paleoclimatic implications of late Ordovician vertic
 367 paleosols, Juniata formation, southern Appalachians: *Journal of Sedimentary Petrology* 62, 71–83.
- 368 Driese, S.G., Simpson, L.E., Erikson, A.K., 1995. Redoximorphic paleosols in alluvial and lacustrine deposits,
 369 1.8 GA Lochnes Formation, Mount Isa, Australia: pedogenic processes and implications for paleoclimate.
 370 *Journal of Sedimentary Research* A65, 675–689.
- 371 Driese, S.G., Mora, C.I., Stiles, C.A., Joeckel, R.M., Nordt, L.C., 2000. Mass-balance reconstruction of a
 372 modern Vertisol: implications for interpreting the geochemistry and burial alteration of paleo-Vertisols.
 373 *Geoderma* 95, 179–204.
- 374 Einsele, G., 1983. Mechanismus und Tiefgang der Verwitterung bei mesozoischen Ton-Mergelsteinen.
 375 *Zeitschrift der Deutschen Geologischen Gesellschaft* 134, 289–315.
- 376 Gasparatos, D., Haidouti, C., Tsagalides, A. and Tarenides, D., 2002. Mineralogical composition of Fe-Mn
 377 concretions in an imperfectly drained Alfisol. *Proceedings of 9th Panhellenic Soil Congress, Hellenic Soil*
 378 *Science Society* 1, 527–535.
- 379 Gasparatos D, Haidouti C, Tarenidis D., 2004. Characterization of iron oxides in Fe-rich concretions from an
 380 imperfectly drained Greek soil: a study by selective-dissolution techniques and X-ray diffraction. *Archives of*
 381 *Agronomy and Soil Science* 50, 485–493.
- 382 Gasparatos, D., 2012. Fe–Mn Concretions and Nodules to Sequester Heavy Metals in Soils. Lichtfouse, E.,
 383 Schwarzbauer, J., Robert, D. (eds.): *Environmental Chemistry for a Sustainable World* 2, 444–474.
- 384 Genise, J.F., Belloso, E.S., Gonzalez, M.G., 2004. An approach to the description and interpretation of
 385 ichnofabrics in paleosols. In: McIlroy, D. (ed.): *The Application of Ichnology to Palaeoenvironmental and*
 386 *Stratigraphic Analysis*. Geological Society of London, Special Publications 228, 355–382.
- 387 Gregory, M.R., Martin, A.J., Campbell, K.A., 2004. Compound trace fossils formed by plant and animal
 388 interactions: Quaternary of northern New Zealand and Sapelo Island, Georgia (USA). *Fossils and Strata* 51, 88–
 389 105.
- 390 Goldenfeld, N., Chan, P.-Y., Veysey, J., 2006. Dynamics of precipitation pattern formation at geothermal hot
 391 springs. *Physical Review Letters* 96, 254–501.
- 392 Hasiotis, S.T., 2002. *Continental Trace Fossils*. SEPM, Short Course Notes Number 51, Tulsa, Oklahoma. 132 p.

- 393 Hasiotis S.T., Mitchell C.E., 1993. A comparison of crayfish burrow morphologies: Triassic and Holocene fossil,
 394 paleo- and neo-ichnological evidence, and the identification of their burrowing signatures. *Ichnos*, 2, 291–314.
- 395 Hasiotis, S.T., Bourke, M.C., 2006. Continental trace fossils and museum exhibits: displaying burrows as
 396 organism behaviour frozen in time. *Geological Curator* 5, 211–226.
- 397 Hildenbranda, A., Uraib, J.L., 2003. Investigation of the morphology of pore space in mudstones – first results.
 398 *Marine and Petroleum Geology* 20, 1185–1200.
- 399 Howard, J.D. Frey, R.W., 1984. Characteristic trace fossils in nearshore to offshore sequences, Upper Cretaceous
 400 of east-central Utah. *Canadian Journal Earth Science* 21, 200–219.
- 401 Jaeger, J.J., Marivaux, L., Salem, M., Bilal, A.A., Benammi, M., Chaimanee, Y., Düringer, Ph., Marandat, B.,
 402 Métais, E., Schuster, M., Valentin, X., Brunet, M., 2010a. New rodent assemblages from the Eocene Dur At-
 403 Talah escarpment (Sahara of central Libya): systematic, biochronological, and Palaeobiogeographical
 404 implications. *Zoological Journal of Linnean Society* 160, 195–213.
- 405 Jaeger, J.J., Beard, K.C., Chaimanee, Y., Salem, M.J., Benammi, M., Hlal, O., Coster, P., Bilal, A.A., Düringer,
 406 Ph., Schuster, M., Valentin, X., Marandat, B., Marivaux, L., Métais, E., Hammuda, O., Brunat, M., 2010b. Late
 407 middle Eocene epoch of Libya yields earliest known radiations of African anthropoids. *Nature* 467, 1095–1099.
- 408 Jaillard, B., Guyon, A. and Manrin, A.F., 1991. Structure and composition of calcified roots and their
 409 identification in calcareous soils. *Geoderma*, 50, 197–210.
- 410 Kessler, M.A., Werner B.T., 2003. Self-organization of sorted patterned ground. *Science* 299, 380–383.
- 411 Kishné, A. Sz., Morgan, C.L.S., Miller, W.L., 2009. Vertisol Crack Extent Associated with Gilgai and Soil
 412 Moisture in the Texas Gulf Coast Prairie. *Soil Science Society of America Journal* 73, 1122–1231.
- 413 Klappa, C.F., 1980. Rhizoliths in terrestrial carbonates: classification, recognition, genesis, and significance:
 414 *Sedimentology* 26, 613–629.
- 415 Kovda, I., Goryachkin, S., Lebedeva, M., Chizhikova N., Kulikov, A., Badmaev, N., 2017. Vertic soils and
 416 Vertisols in cryogenic environments of southern Siberia, Russia. *Geoderma* 288, 184–195.
- 417 Kraus, M.J., 1998. Development of potential acid sulfate paleosols in Paleocene floodplains, Bighorn Basin,
 418 Wyoming, USA: Palaeogeography, Palaeoclimatology, Palaeoecology 144, 203–224.
- 419 Kraus, M.J., Aslan, A., 1993. Eocene hydromorphic paleosols: significance for interpreting ancient floodplain
 420 processes. *Journal of Sedimentary Petrology* 63, 453–463.
- 421 Kraus, M.J., Hasiotis, S.T., 2006. Significance of different modes of rhizolith preservation to interpreting
 422 paleoenvironmental and paleohydrologic settings: examples from Paleogene paleosols, Bighorn Basin,
 423 Wyoming, U.S.A. *Journal of Sedimentary Research* 76, 633–646.
- 424 Li, J.H., Zhang, L.M., Wang, Y., Fredlund, D.G., 2009. Permeability tensor and representative elementary
 425 volume of saturated cracked soil. *Canadian Geotechnical Journal* 46, 928–942.
- 426 Manceau, A., Drits, V.A., Lanson, B., Chateigner, D., Wu, J., Huo, D., Gates, W.P., Stucki, J.W., 2000.
 427 Oxidation reduction mechanism of iron in dioctahedral smectites. II. Crystal chemistry of reduced Garfield
 428 nontronite. *American Mineralogist* 85, 153–172.
- 429 Mack, G.H., James, W.C., Monger, H.C., 1993. Classification of paleosols: Geological Society of America
 430 Bulletin 105, 129–136.
- 431 Miller, W.L., Kishne, A.S., Morgan, C.L., 2010. Vertisol morphology, classification, and seasonal cracking
 432 patterns in the Texas Gulf coast prairie. *Soil Horizons* 51, 10–16.
- 433 Moh, H.H., Chong, V.C., Sasekumar, A., 2015. Distribution and burrow morphology of three sympatric species
 434 of *Thalassina* mud lobsters in relation to environmental parameters on a Malayan mangrove shore. *Journal of Sea*
 435 *Research*, 95, 75–83.
- 436 Monaco, P., 2000. Decapod burrows (*Thalassinoides*, *Ophiomorpha*) and crustacean remains in the Calcari
 437 Grigi, Lower Jurassic, Trento platform (Italy). 1st Workshop on Mesozoic and Tertiary decapod crustaceans
 438 (VI), 293–301.
- 439 Mondol, N.H., Bjorlykke, K., Jahren, J., 2008. Experimental compaction of clays: relationship between
 440 permeability and petrophysical properties in mudstones. *Petroleum Geoscience* 14, 319–337.
- 441 Moussavi-Harami, R., Mahboubi, A., Nadjafi, M., Brenner, R.L., Mortazavi, M., 2009. Mechanism of calcrete
 442 formation in the Lower Cretaceous (Neocomian) fluvial deposits, northeastern Iran based on petrographic,
 443 geochemical data. *Cretaceous Research* 30, 1146–1156.
- 444 Muller, J.-P., Bocquier, G., 1986. Dissolution of kaolinites and accumulation of iron oxides in lateritic-
 445 ferruginous nodules: mineralogical and microstructural transformations. *Geoderma* 37, 113–136.
- 446 Nascimento, D., L., Batezelli, A., Ladeira, F.S., 2019. The paleoecological and paleoenvironmental importance
 447 of root traces: plant distribution and topographic significance of root patterns in upper cretaceous paleosols.
 448 *Catena* 172, 789–806.
- 449 Ollier, C.D., 1971. Causes of spheroidal weathering. *Earth-Sciences Reviews* 7, 127–141.
- 450 Pipujol, M.D., Buurman, P., 1994. The distinction between ground-water gley and surface-water gley
 451 phenomena in Tertiary Paleosols of the Ebro Basin, NE Spain: Palaeogeography, Palaeoclimatology,
 452 Palaeoecology 110, 103–113.

- 453 Rayhani, M.H.T., Yanful, E.K., Fakher, A., 2008. Physical modeling of desiccation cracking in plastic soils.
 454 Engineering Geology 97, 25–31.
- 455 Retallack, G.J., 1983. Late Eocene and Oligocene paleosols from Badlands National Park, South Dakota:
 456 Geological Society of America, Special Paper 193, 82 p.
- 457 Sadek, S., Sultan, R., 2011. Liesegang patterns in nature: A diverse scenery across the sciences, a review paper,
 458 Research Snapshot, 37/661, 1–43.
- 459 Schwertmann, U., 1993. Relations between iron oxides, soil colour, and soil formation: Journal of Soil Science
 460 31, 51–69.
- 461 Schwertmann, U., Taylor, R.M., 1989. Iron oxides, in Dixon, J.B., Weed, S.B., (eds.): Minerals in Soil
 462 Environments. Soil Science Society of America p. 379–438.
- 463 Seilacher, A., 2007. Trace fossil analysis. Springer Verlag, Heidelberg, 226 p.
- 464 Smith, J.J., Hasiotis, S.T., Woody, D.T., Kraus, M.J., 2008. Paleoclimatic implications of crayfish-mediated
 465 prismatic structures in paleosols of the Paleogene Willwood formation, Bighorn basin, Wyoming, U.S.A. Journal
 466 of Sedimentary Research 78, 323–334.
- 467 Soil Survey Staff, 1998. Keys to Soil Taxonomy, 8th edn. US Government Printing Office, Washington DC, 324
 468 p.
- 469 Sridharan, A., Allam, M.M., 1982. Volume change behaviour of desiccated soils. Proceedings of ASCE. Journal
 470 of the Geotechnical Engineering Division, 108, 1057–1071.
- 471 Thompson, A.E., Stokes, W.L., 1970. Stratigraphy of the San Rafael Group, southwest and south-central Utah.
 472 Utah Geological and Mineralogical Survey Bulletin 87, 53 p.
- 473 Veneman P.L.M., Vepraskas, M.J., Bouma, J., 1975. The physical significance of soil mottling in a Wisconsin
 474 toposequence. Geoderma, 15, 103–118.
- 475 Vepraskas, M.J., 1994. Redoximorphic features for identifying aquic conditions: North Carolina Agricultural
 476 Research Service, Technical Bulletin 301, 33 p.
- 477 Wang, Y., Chan, M.A., Merino, E., 2015. Self-organized iron-oxide cementation geometry as an indicator of
 478 paleo-flows. Scientific Report, srep10792, 1–15 p.
- 479 Wight, A.W.R., 1980. Paleogene vertebrate fauna and regressive sediments of Dur At Talah, southern Sirt Basin,
 480 Libya. In: Salem, M.J., Burwell, M.T. (eds.): The Geology of Libya, vol. I. Academic Press, London, p. 309-325.
- 481 Yuen, K., Graham, J., Janzen, P., 1998. Weathering-induced fissuring and hydraulic conductivity in a natural
 482 plastic clay. Canadian Geotechnical Journal 35, 1101–1108.
- 483 Zhang, M., Karathanasis, A.D., 1997. Characterization of iron–manganese concretions in Kentucky alfisols with
 484 perched water tables. Clays and Clay Minerals 45, 428–439.

485
 486 **Figure captions**
 487

488 Fig. 1: Location and geological section; a) map of Libya shows the location of the area of study (the
 489 rectangle); b) the representative section of New Idam Unit, shows the position of the mudstone hosting
 490 the redoximorphic pedo-turbations; c) outcrop view of the studied mudstone.

491 Fig. 2: The variations of the mudstone's fractural fabric; a) initial open fractures separating vertical
 492 mud blocks; b) disintegration of vertical mud blocks into smaller peds. Circular and semi-cylindrical
 493 mud masses was formed (dashed green and orange lines); c) base of large mudstone block shows
 494 different generation of cracks; d) initial phases of staining of the mud blocks, Fe-oxide concentrates
 495 adjacent to the crack walls (e.g., arrows); e) semi-cylindrical mud mass shows subordinate phase of
 496 (horizontal) fracturing; f) aggregated sub- (vertical) fracture with branchings, morphologically
 497 comparable to root tracks; g) aggregated (vermicular) network of fractures, imitating bioturbations; h)
 498 diagonally intersected short-spaced fractures seen only in the host mud.

499 Fig. 3: Possibilities of the patterns of the fractures as exhibited by the host mudstone; a) longitudinal,
 500 straight and irregular fractures. Control of fractures on redox forms is remarkable in a, b; b) similar
 501 representation of the redox feature in a different manner; c, d) image and drawing illustrate the circular
 502 cracks dominated the lower reaches of the bed; e) composite straight and circular fractures
 503 producing/separating subcircular masses of variable sizes, internal concentric rings; f) vermicular
 504 fabric, caused by the combination of fractures and mud aggregation. Scale bar: a, b 5 cm; c, d and e 2
 505 cm; f 1.5 cm.

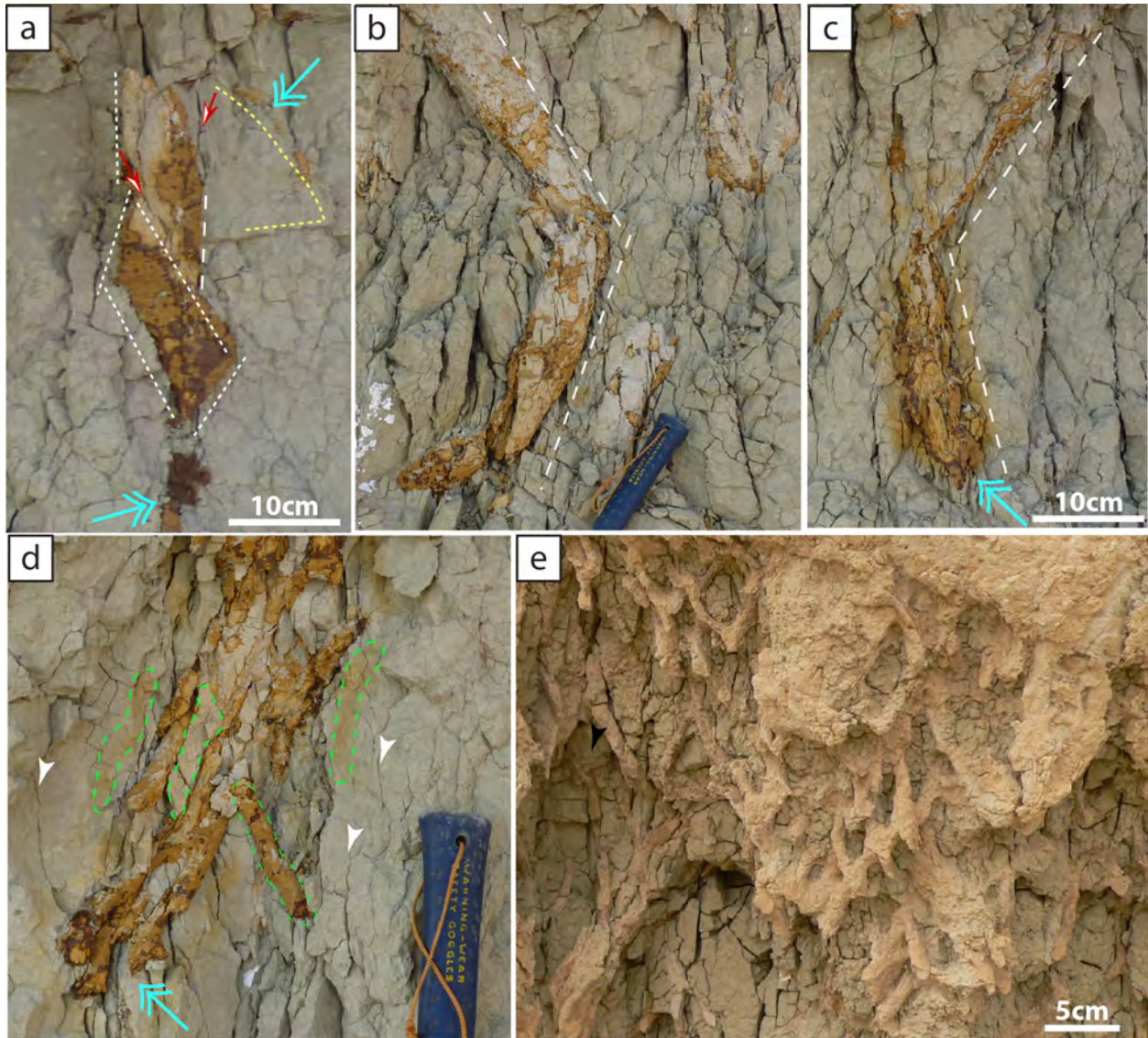
506 Fig. 4: The appearance of the studied structures in the outcrop; a, b) general views shows the change
507 from crowded network of small tubules to larger shafts below (inconsistent with roots); c–f) shafts
508 from different locations but of the same horizontal level, unambiguously oriented parallel.
509 Excavation/penetration cannot not be proven in these forms. The brown Fe-oxides engulf physically
510 intact mudstone masses. Lines highlight parallelism. In the images (c) and (e) the scale is the finger
511 and the hand respectively.

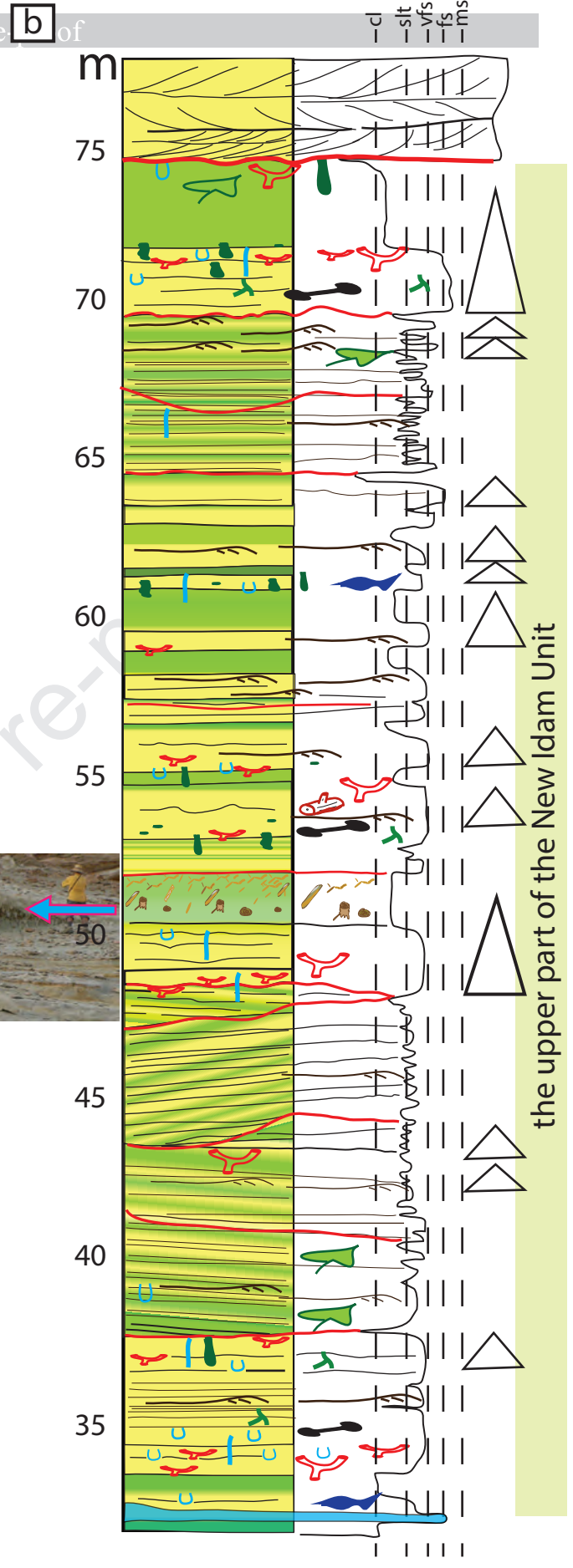
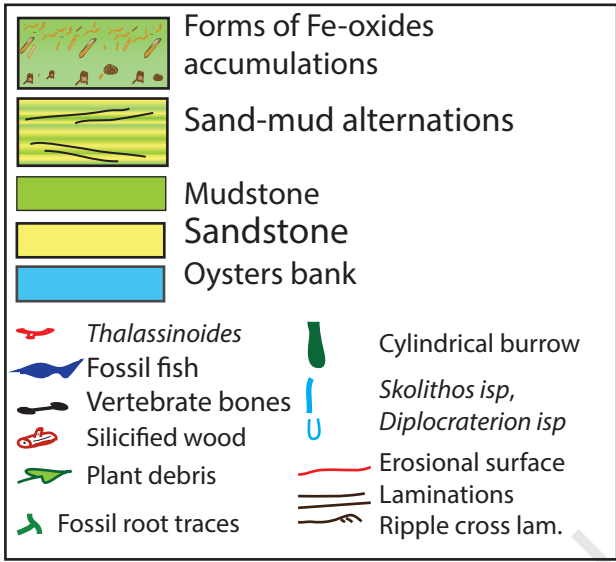
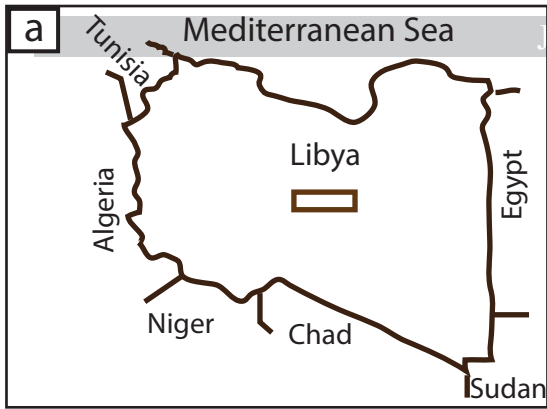
512 Fig. 5: The occurrence pattern and morphology of the hosted structures; a) wedge shaped rectangular
513 mud block stained/coated by Fe-oxide. Red arrows for slickenside faces, blue arrows point to the
514 initial oxidation spots along fractures; b, c) differentially pigmented mud blocks, notice the privileged
515 (fracture-controlled) diversion angle (dashed lines). The interior preserves the same fractures as that of
516 the ambient mud; d) semi-tubules within a fractured block, oxidized ones are similar to that which are
517 partially oxidized. The halos in the vicinity, have nearly the same shape, size and more or less
518 orientations, arrow heads point to microfractures that might be in relation. The blue arrows point to the
519 likely descending Fe-oxides growth; e) close-up view of the rectangle in Figure (4b). It shows shortly
520 spaced diagonally attached straight segments (individual tubules), of which the intensity and
521 orientations are comparable to that of the associated cracks (comparable also to the fracture's pattern
522 in Figure (2h). Hammer handle for scale in (b) and (d).

523 Fig. 6: The irregularly cylindrical-shaped simple and composite vertical forms; a) appearance in the
524 outcrop; b) large tube composed of smaller tubules (comparable to the circular fractures in Fig. 3c-e),
525 another example of such composite shafts is presented by the image (c); d) subvertical cylindrical
526 body with descendant tubular/tabular appendages attached to it, this is shown also in a, b (the arrows).
527 Some are not attached (dashed circles in b, c). The red arrow head points to a tabular, aggregated
528 fracture zone. It is morphologically comparable to the adjacent, long oxidized appendages.

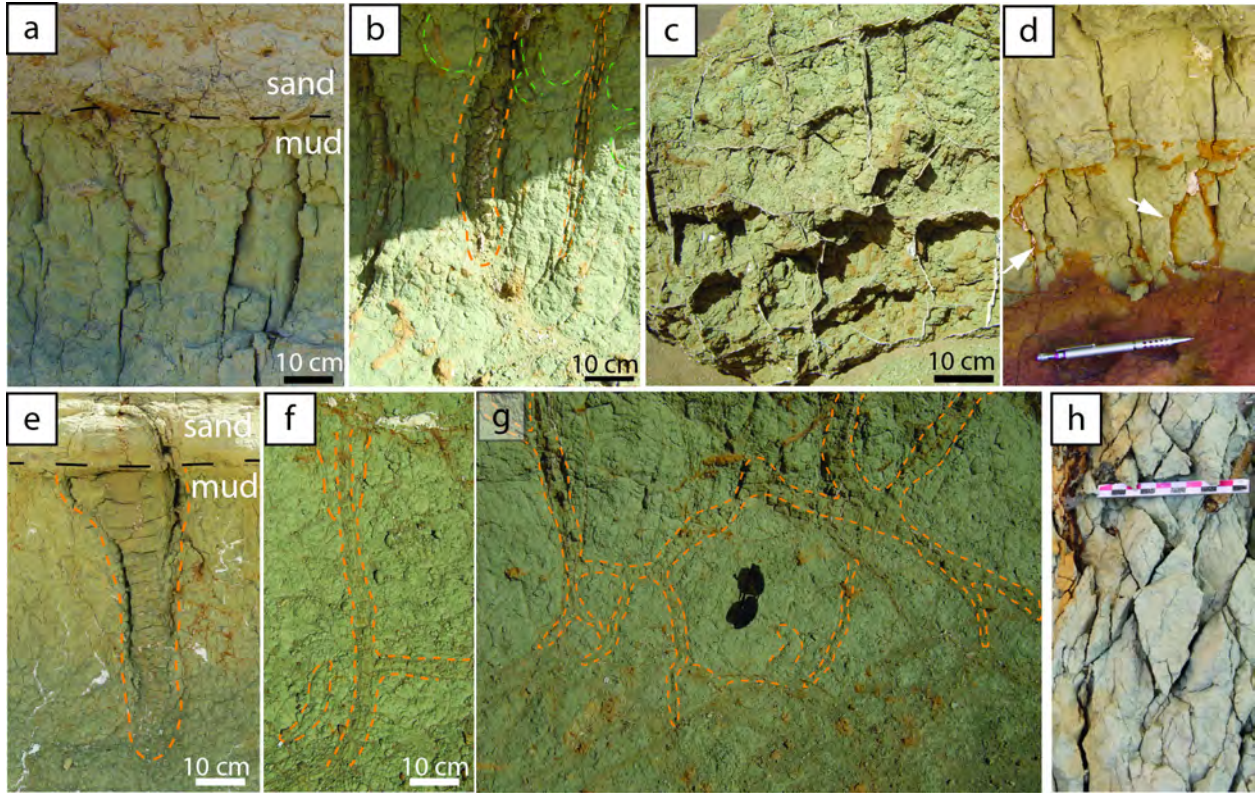
529 Fig. 7: Practical proof of the physical template-based Fe-oxides morphologies; a, b) image and
530 illustrative sketch suggesting that the precipitation is guided by the concentric cracks (compare Fig.
531 3c-d). The arrows point to the incomplete cylindrical growth as guided by the circular fracture. Such
532 arc (arrows) would continue to form (a perfect) vertical tubular body, if the reaction had not been
533 stopped. The same way, regardless of diameter, the completed rings (solid lines) had been originated
534 by overprinting the dashed ones; c) this image proposes an example of the fabrication of tubular forms
535 based on a pre-exist physical (fabric) template. Oxidation (brown) and reduction (gray) occurred
536 adjacently, the fractures are the visible control for the redistribution of the iron oxides. The red dashed
537 lines are for the roughly shaped unoxidized tubes, the solid red lines are for the reshaping by the Fe-
538 oxides growth, black lines point to the fine internal (subordinate) cracks. The general view of the
539 image (c) is the square in Figure (3b); d) subvertical shaft body shows that the Fe-oxide accumulation
540 is supervised by the pre-existed fractures (straight green lines). Further Fe-oxide accumulation would
541 mask these details and would result in a complete cylindrical shape.

542

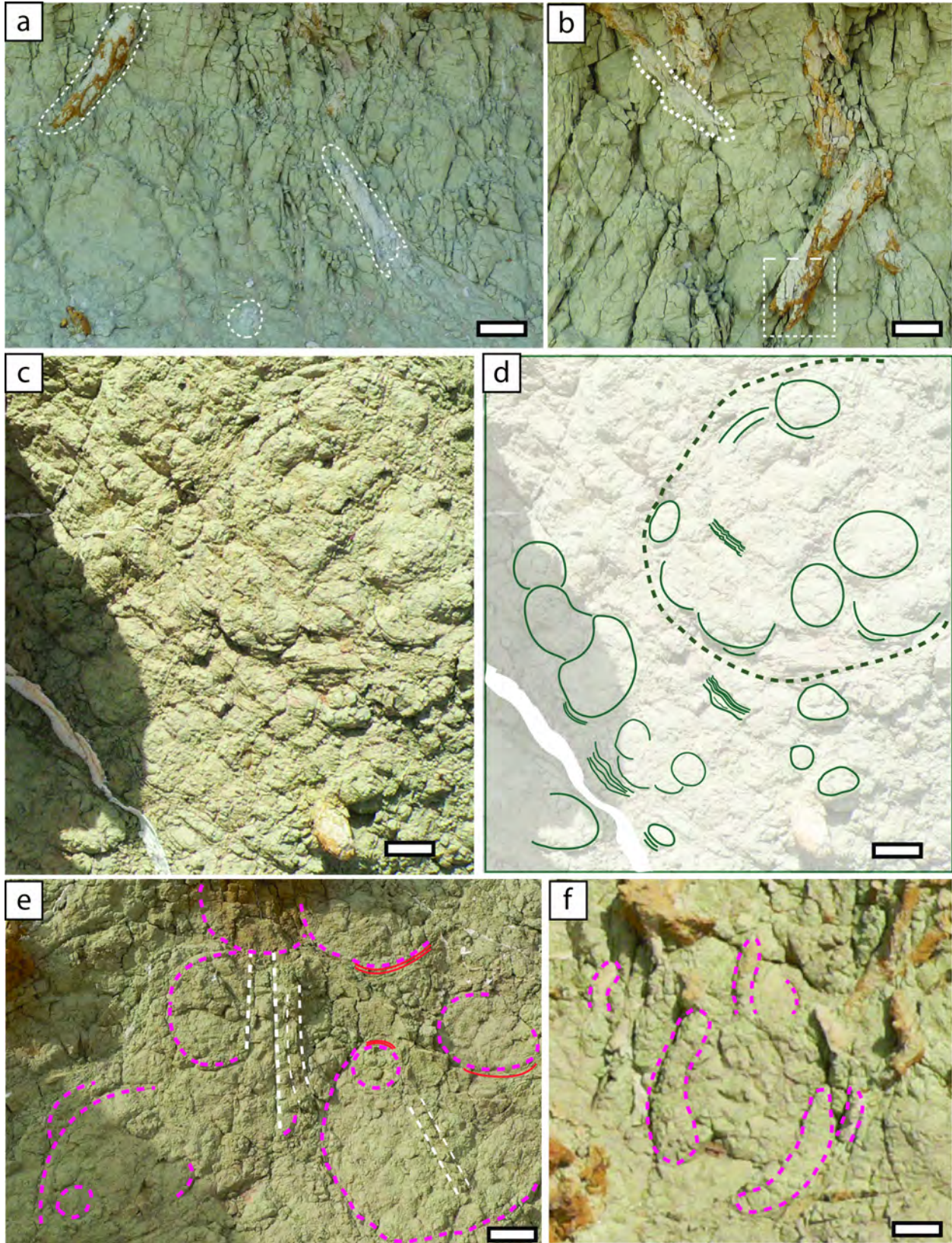


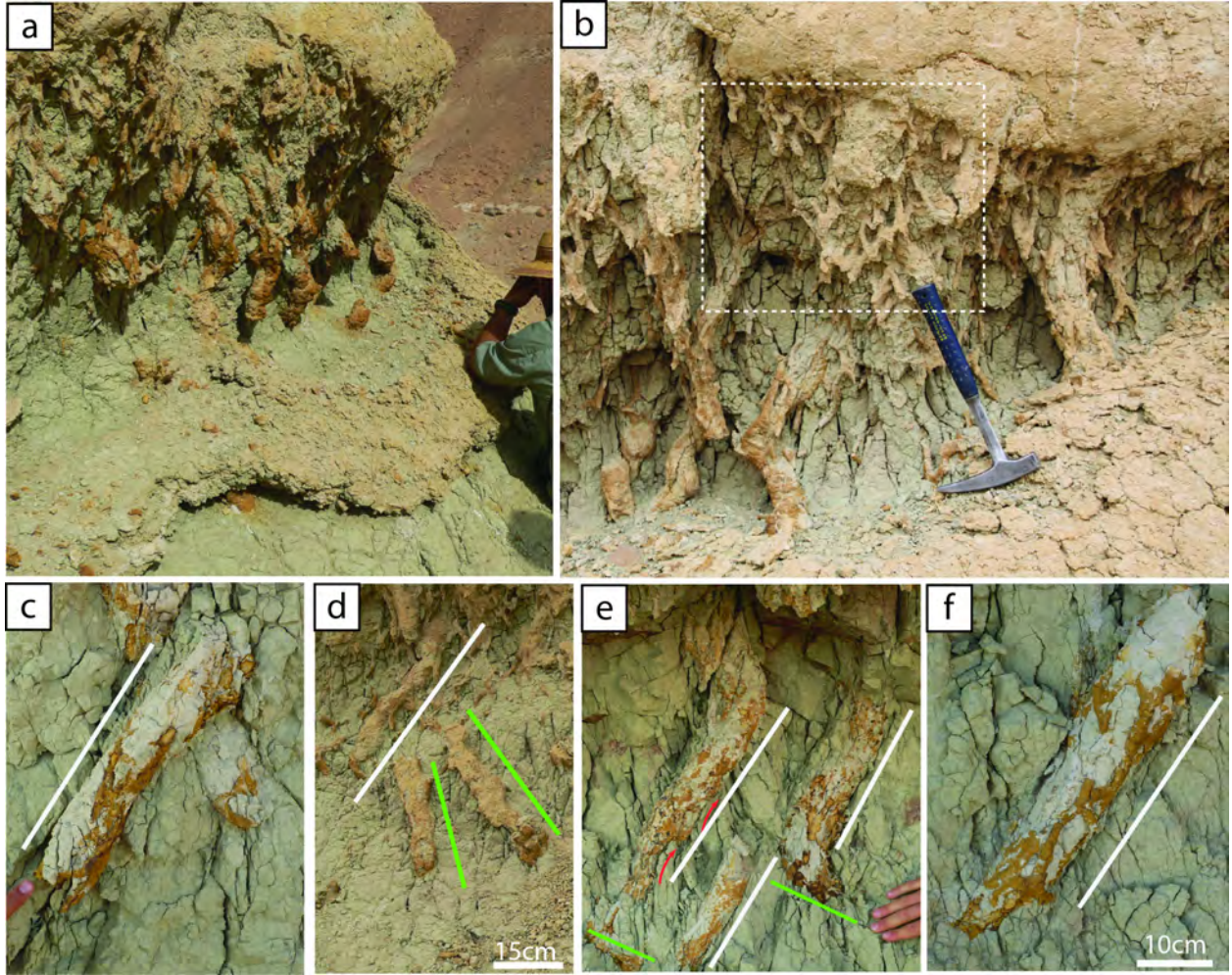


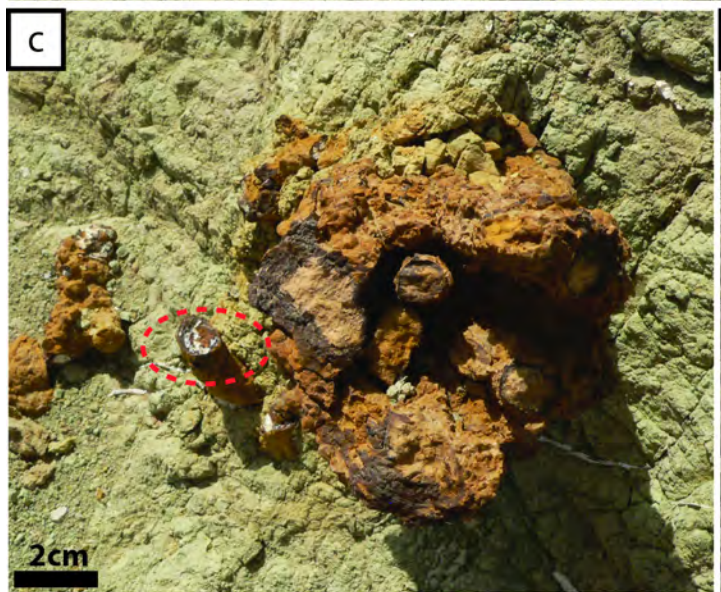
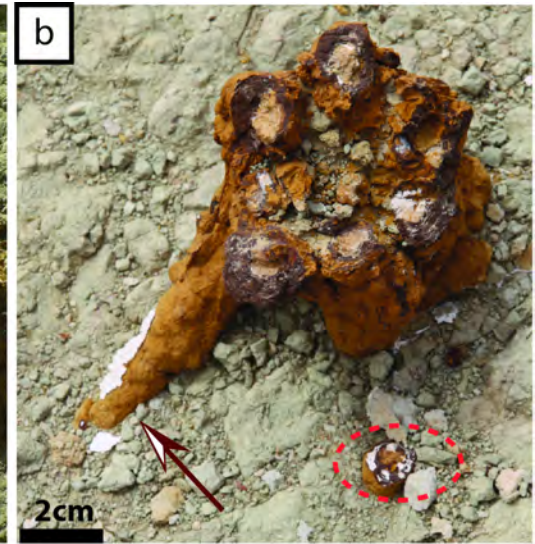
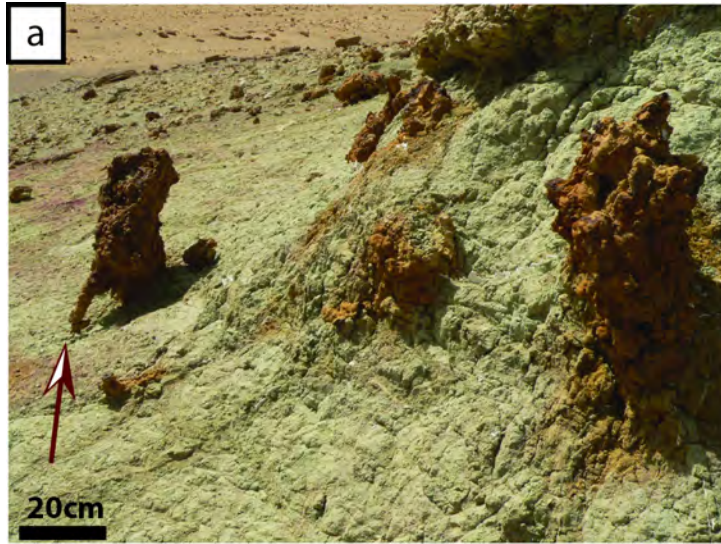
the upper part of the New Idam Unit

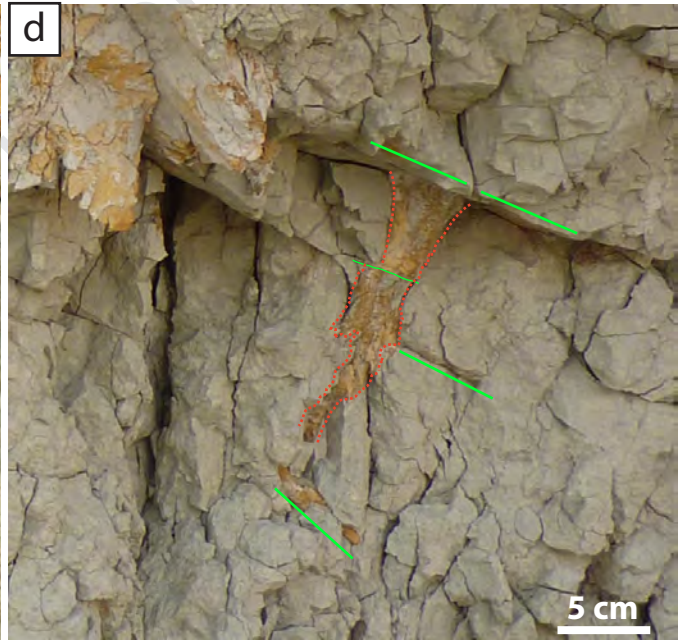
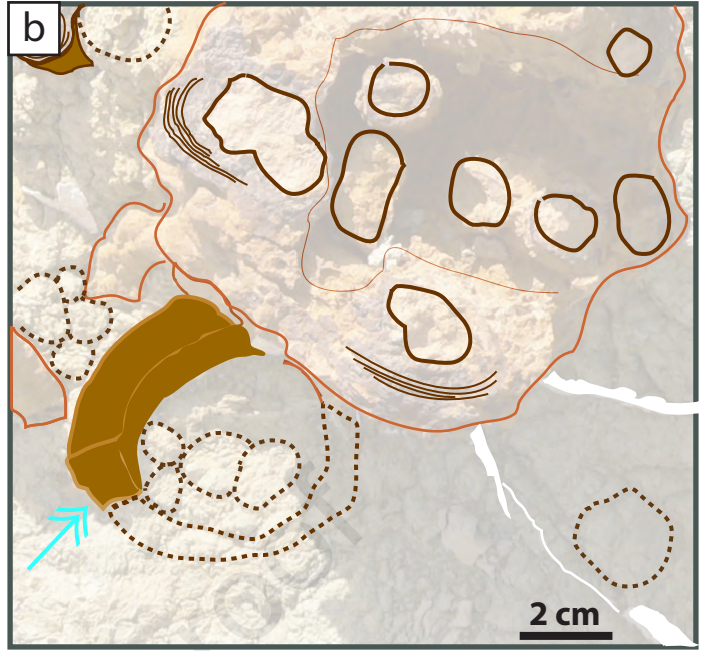
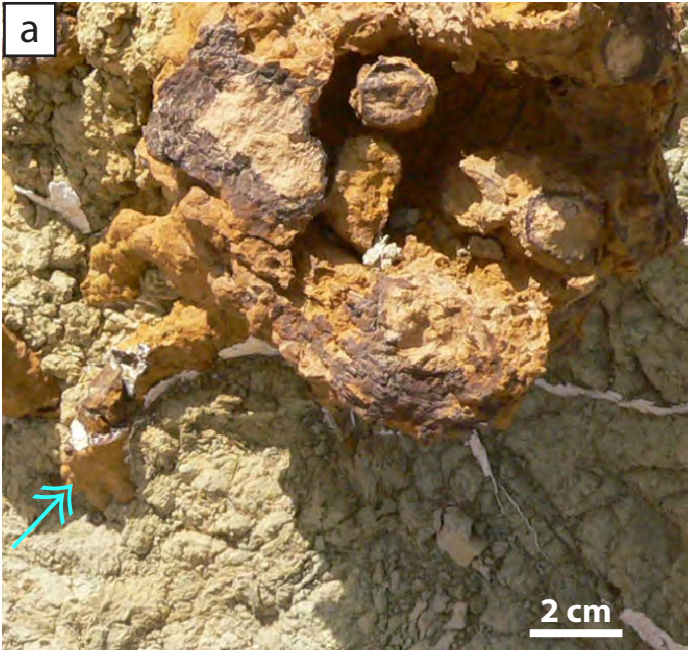


Journal Pre-proof









Highlights

- Mudstone's physical fabric creates trace fossil-like features
- The recognition criteria of paleosols are useful as indicators of paleoclimate
- Redox processes in paleosols may cause misleading geological interpretation
- Subaerial exposure in the Eocene of Sirt basin indicated by pedogenic structures

Journal Pre-proof

Declaration of interests

The authors declare that they have no known competing financial interests or personal relationships that could have appeared to influence the work reported in this paper.

The authors declare the following financial interests/personal relationships which may be considered as potential competing interests:

Dr. Ashour Abouessa on behave of the authors

29/04
2020 